''Shim pulses'' for NMR spectroscopy and imaging

Daniel Topgaard*†, Rachel W. Martin*, Dimitris Sakellariou‡, Carlos A. Meriles§, and Alexander Pines*

*Materials Sciences Division, Ernest Orlando Lawrence Berkeley National Laboratory and Department of Chemistry, University of California, Berkeley, CA 94720; ‡Departement de Recherche sur l'État Condensé, les Atomes et les Molécules, Direction des Sciences de la Matière, Commissariat à l'Energie Atomique Saclay, Service de Chimie Moléculaire, F-91191 Gif-sur-Yvette Cedex, France; and §Department of Physics, City College of New York, New York, NY 10031

Contributed by Alexander Pines, November 9, 2004

A way to use adiabatic radiofrequency pulses and modulated magnetic-field gradient pulses, together constituting a ''shim pulse,'' for NMR spectroscopy and imaging is demonstrated. These pulses capitalize on phase shifts derived from probe gradient coils to compensate for nonlinear intrinsic main magnetic field homogeneity for spectroscopy, as well as for deviations from linear gradients for imaging. This approach opens up the possibility of exploiting cheaper, less-than-perfect magnets and gradient coils for NMR applications.

adiabatic | modulated gradient | MRI | pulse sequence | numerical optimization

Traditional NMR spectroscopy and imaging experiments are performed under conditions in which the main, radiofrequency (RF), and gradient fields are as homogeneous as possible, resulting in NMR spectra with narrow resonance lines and images with well defined spatial encoding. The main field, which is usually produced by a superconducting solenoid, is made more homogeneous by adjusting the currents applied to a large set of coils (the so-called ''shim'' coils), whereas the homogeneity of the RF and gradient fields are assured by sophisticated design methods for the coil-winding patterns. The field homogeneity can also be improved by increasing the size of the hardware components in comparison with the active sample volume. The shape of the magnetic field is related directly to the geometry of the conductors producing the field.

In this article, we propose and demonstrate a methodology to reshape the effective magnetic field that the spins experience by using modulated gradient pulses and adiabatic RF pulses. Effectively, the spins behave as though they precess in a magnetic field with a different shape than the shape that is intrinsic to the coil and magnet design. The shape of this apparent field is controlled by the time dependence of the gradient coil currents as well as phase and amplitude modulation of the RF magnetic field. The idea of using adiabatic RF pulses to modulate the phase of the transverse magnetization with spatial resolution stems from the work by Meriles *et al.* (1) and other work dealing with the *ex situ* methodology aiming for chemical-shift-resolved NMR with single-sided or inside-out magnet designs (2–6). Whereas this earlier approach depended entirely on spatial matching between the inhomogeneity of the main and RF magnetic fields, the methodology presented here can be designed to either capitalize on favorable RF inhomogeneity or to be insensitive to it.

We suggest the name ''shim pulse'' for an RF- and gradient-pulse sequence inducing a phase modulation that cannot be described as a linear combination of the effects from the fields intrinsic to the coil geometries. Shim pulses may be used to correct for artifacts originating from less-than-perfect magnets and gradient coils and, in this way, relax some of the constraints for hardware design.

A related method for obtaining resolved NMR spectra from samples in an inhomogeneous magnetic field was demonstrated recently as an extension of the single-shot 2D NMR technique by Frydman and coworkers (7–9). In this approach, gradients and shaped RF pulses are used to sequentially excite different slices of the sample. The excitation RF pulses impose a phase shift that is adjusted to cancel the effect of the inhomogeneity at the time of signal detection (10).

After briefly describing the theory and outlining the numerical methods for shim-pulse design, we demonstrate the potential of this approach with three experiments. First, two gradient coils producing two orthogonal linear magnetic fields were used to induce a 2D saddle-shaped phase shift, which is visualized by an imaging method. Second, a gradient coil producing a linear magnetic field was used to ''shim'' the NMR spectrum from a sample in a magnetic field with a quadratic inhomogeneity. Last, the influence of a gradient coil producing a field with linear and cubic components was reshaped to provide purely linear phase encoding and a nondistorted image.

Methods

Theory. The objective was to design a pulse that modulates the phase $\phi(\mathbf{r})$ of the transverse magnetization by an amount depending on position $\mathbf{r}$, where the functional form of $\phi(\mathbf{r})$ is under software control. To constitute a robust experimental method, $\phi(\mathbf{r})$ should be insensitive to frequency offset, including offset due to chemical shift σ, and RF amplitude misset within reasonable ranges. We limit this discussion to noninteracting spins 1/2 with gyromagnetic ratio γ in a strong main magnetic field, implying that the direction of quantization is unaffected by the applied gradients.

If signal damping originating from relaxation and diffusion is neglected, the transformation of the local magnetization vector $\mathbf{m}(\mathbf{r}, t)$ during a general RF- and gradient-pulse sequence lasting a time t_p can be written as follows:

$$\mathbf{m}(\mathbf{r},\ t = t_p) = \mathbf{R}(\mathbf{r})\mathbf{m}(\mathbf{r},\ t = 0). \qquad [1]$$

$\mathbf{R}(\mathbf{r})$ is a rotation matrix, which depends on the time dependence of the local Larmor frequency $\omega_0(\mathbf{r}, t)$, local nutation frequency $\omega_1(\mathbf{r}, t)$, RF phase $\varphi(t)$, and RF carrier frequency ω_{RF} during the pulse sequence. On modern NMR spectrometers, shaped RF and gradient pulses are implemented as a sequence of square pulses with constant RF amplitude, RF phase, and gradient amplitudes. The total rotation matrix for a shaped pulse can be calculated by sequential multiplication of the rotation matrices for the individual square pulses given in ref. 11, for example.

The local nutation frequency is given by the following:

$$\omega_1(\mathbf{r}, t) = -\gamma B_1(\mathbf{r}) A_{RF}(t), \qquad [2]$$

where $A_{RF}(t)$ is the time-dependent relative RF amplitude and $B_1(\mathbf{r})$ is the maximum local RF amplitude. It is convenient to express the local Larmor frequency offset $\Delta\omega_0(\mathbf{r}, t) = \omega_0(\mathbf{r}, t) - \omega_{RF}$ as follows:

Abbreviation: RF, radiofrequency.

†To whom correspondence should be addressed at: Department of Physical Chemistry 1, Lund University, P.O. Box 124, SE-221 00 Lund, Sweden. E-mail: daniel.topgaard@fkem1.lu.se.

www.pnas.org/cgi/doi/10.1073/pnas.0408296102

$$\Delta\omega_0(\mathbf{r}, t) = -\gamma(1 - \sigma)\left[B_0(\mathbf{r}) + \sum_{n=1}^{N} B_{0,n}(\mathbf{r})A_n(t) \right] - \omega_{\mathrm{RF}}, \quad [3]$$

where $B_0(\mathbf{r})$ is the magnetic field produced by the main magnet, and $B_{0,n}(\mathbf{r})$ are the maximum magnetic fields originating from the N auxiliary "gradient" coils. $A_n(t)$ are the relative amplitudes of the field from each of these coils. $B_1(\mathbf{r})$, $B_0(\mathbf{r})$, and $B_{0,n}(\mathbf{r})$ are given by the coil geometries, neglecting sample-induced field distortions, whereas $\varphi(t)$, $A_{\mathrm{RF}}(t)$, and $A_n(t)$ are controlled by the spectrometer software. The ω_{RF} value is constant and close to the average value of $\gamma B_0(\mathbf{r})$ in the region of space from which the NMR signal is detected.

If the rotation matrix is expressed in Cartesian coordinates, the deviation χ^2 from ideal pulse performance can be defined as follows:

$$\begin{aligned}\chi^2(\phi(t), A_{\mathrm{RF}}(t), A_1(t), \ldots, A_N(t)) &= \sum_i w_1[\arg(R_{xx}(\mathbf{r}_i) + iR_{yx}(\mathbf{r}_i)) - \phi(\mathbf{r}_i)]^2 \\ &+ w_1[\arg(R_{yy}(\mathbf{r}_i) - iR_{xy}(\mathbf{r}_i)) - \phi(\mathbf{r}_i)]^2 \\ &+ w_2[|R_{xx}(\mathbf{r}_i) + iR_{yx}(\mathbf{r}_i)| - 1]^2 \\ &+ w_2[|R_{yy}(\mathbf{r}_i) - iR_{xy}(\mathbf{r}_i)| - 1]^2 \\ &+ w_3[R_{zz}(\mathbf{r}_i) - 1]^2, \end{aligned} \quad [4]$$

where w_1, w_2, and w_3 are weighting parameters. The w_1-weighted terms quantify the deviation from the target phase shift, and the terms weighted by w_2 and w_3 describe the loss of transverse and longitudinal magnetization. The values of the weighting parameters reflect the relative importance of the different terms, but they are generally of the same order of magnitude. The definition of χ^2 in Eq. **4** is only one of several different possibilities, but we find this version particularly transparent with respect to the desired result (i.e., a pure rotation of the magnetization around the z axis).

Finding the functions $\varphi(t)$, $A_{\mathrm{RF}}(t)$, and $A_n(t)$ that minimize χ^2 under the conditions given by $B_1(\mathbf{r})$, $B_0(\mathbf{r})$, and $B_{0,n}(\mathbf{r})$ is a straightforward nonlinear least-squares problem. The functions $\varphi(t)$, $A_{\mathrm{RF}}(t)$, and $A_n(t)$ should be well behaved in the sense that implementation on a standard NMR spectrometer is feasible. This condition can be assured by either including a term penalizing unrealistic modulation functions in the definition of χ^2 or by expressing the modulation as a smooth analytical function with a limited number of adjustable parameters. The calculation of χ^2 should also be performed over a range of B_0 offsets and B_1 amplitude missets to guarantee a certain degree of robustness. Note that favorable B_1 gradients could be used in the manner of the *ex situ* methodology (1).

Let us assume that we have designed a pulse that gives rise to the desired $\phi(\mathbf{r})$. If we sample the NMR signal at the midpoint of the free precession delays in a train of interleaved shim pulses with length t_{p} and free-precession delays with length t_{dw}, it appears as though the spins are precessing under the influence of the B_0 offset, including chemical shift, for a time t_{dw} in an apparent field of strength as follows:

$$B_{0,\mathrm{app}}(\mathbf{r}) = B_0(\mathbf{r}) - \frac{\phi(\mathbf{r})}{\gamma t_{\mathrm{dw}}}. \quad [5]$$

This fact means that the apparent field experienced by the spins can be controlled by the time modulation of the RF field and the auxiliary coil currents. These modulation functions can then be adjusted to make the field appear to be homogeneous for spectroscopy applications or to have a constant gradient for imaging purposes. The desired field profile can be achieved, although none of the hardware components or any linear combination of them, provide constant main field or linear gradient field. This description disregards J couplings and signal damping due to relaxation and diffusion during t_{p}.

Pulse Design. As the point of departure for the shim-pulse design, we used the well known fact that an adiabatic full passage applied to transverse magnetization induces a phase shift depending on the frequency offset (12). A second passage reverses this phase shift and restores any longitudinal magnetization to its initial state. However, a residual phase shift will be the result of an adiabatic double passage in the presence of a B_0 inhomogeneity, which is changing between the first and the second passage. Intuitively, it seems possible to tailor the spatial shape of the phase shift by a smooth modulation of the current applied to the coil producing the B_0 inhomogeneity. In the examples given below, we verify this assumption.

For the adiabatic pulses, we chose to use the sech and tanh amplitude and frequency modulation functions (13). The amplitude modulation of $A_n(t)$ was expressed as a sum of M sine functions as follows:

$$A_n(t) = \sum_{m=1}^{M} a_{mn} \sin(m\pi t/t_{\mathrm{p}}), \quad 0 \le t \le t_{\mathrm{p}} \quad [6]$$

where a_{mn} is the amplitude of each sine component. Typically, M was chosen to be between 10 and 20. This approach assures that the modulation is zero at the beginning and end of the pulse and reasonably smooth in between. The pulses were discretized in 200 or 500 steps, depending on the overall pulse length. The set of a_{mn} and, occasionally, t_{p} and the width of the adiabatic frequency sweep were used as adjustable parameters. The pulses were designed to be offset insensitive over a range of ± 5 ppm and independent of B_1 inhomogeneity or missetting in the range of $\pm 25\%$ the nominal value obtained with standard 90° pulse-length calibration. Numerical optimizations were implemented in MATLAB 5.2 (MathWorks, Natick, MA) by using the "constr" routine in the Optimization toolbox. As soon as reasonable initial values of the adjustable parameters were estimated, each pulse optimization took on the order of minutes to hours on a 900-MHz iBook (Macintosh).

Experiments and Results. Experiments were carried out on DMX-300 and Avance-700 spectrometers (Bruker, Billerica, MA) by using Bruker probes with coils producing three orthogonal gradients with a maximum gradient strength of 0.5 T/m at a current of 10 A. The probe for the Avance-700 was a standard high-resolution triple-resonance HCN probe, whereas the probe for the DMX-300 was modified to locate the active volume of the RF coil in a region with nonconstant B_0 gradients. The maximum gradient coil current during the shim pulses was ≈5% of the maximum possible value. The ^{1}H 90° pulse length was ≈10 μs for both spectrometers, corresponding to an RF field strength of 25 kHz. Unless otherwise stated, the relaxation delay was 5 s, and four scans were accumulated throughout. Experimental details for the individual examples are given in the corresponding figure legends.

Saddle-Shaped Phase Shift with Two Orthogonal Linear Gradients. As a first demonstration of the approach, we use two gradient coils producing linear gradients in the x and y directions to induce a saddle-shaped phase shift in the x, y plane. According to the notation given above, these conditions can be expressed as follows:

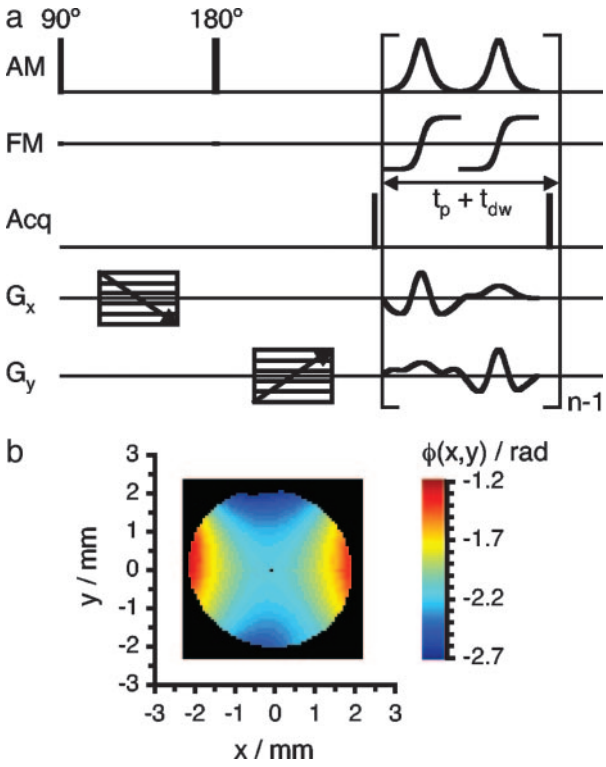

Fig. 1. Visualization of the phase shift induced by a shim pulse. (*a*) Pulse sequence for recording a 2D image of the phase shift $\phi(x, y)$ induced by the shim pulse shown in brackets. The signal from a cylindrical water sample was recorded stroboscopically in windows of length $t_{dw} = 150$ μs during a pulse train with $n = 128$ shim pulses of length $t_p = 1$ ms and an RF sweep width of 40 kHz. The two phase-encoding gradients were incremented in 64 steps each. Fourier transform of the resulting 3D data set yields a ''spectrum'' of the phase shift per shim pulse for each pixel in the image. (*b*) A 2D map of the phase shift is obtained by converting the phase shift at the maximum peak intensity of these spectra to a color scale.

$$\begin{aligned} B_{0,x}(\mathbf{r}) &\propto x \\ B_{0,y}(\mathbf{r}) &\propto y \\ \phi(\mathbf{r}) &\propto x^2 - y^2. \end{aligned} \qquad [7]$$

Note that such a phase shift is impossible when using traditional NMR methods in which the shape of the phase shift is necessarily a linear combination of the shapes of the fields from the gradient coils. A 2D image of the phase shift in the x, y plane was recorded with the pulse sequence in Fig. 1*a* by using a cylindrical water phantom (i.d., 4 mm) aligned along the z direction in a homogeneous B_0 field. This pulse sequence is a modification of a standard chemical shift or B_0 inhomogeneity imaging sequence, yielding an NMR spectrum for each pixel in the image. In the direct dimension, the signal is recorded stroboscopically during a train of shim pulses and free-precession delays. In the indirect dimensions, the strength of the phase encoding gradients are varied. Note that the same gradient coils are used for both the linear phase encoding to obtain the image and the nonlinear phase shifts during detection.

The shim pulse was optimized according to the principles outlined above. As shown in Fig. 1*b*, the resulting phase shift is saddle shaped. The overall constant phase shift is a result of evolution under the offset for a time t_{dw} during the delay in which the signal is recorded. The spins behave as though they evolve under the influence of frequency offset, or chemical shift, in a magnetic field

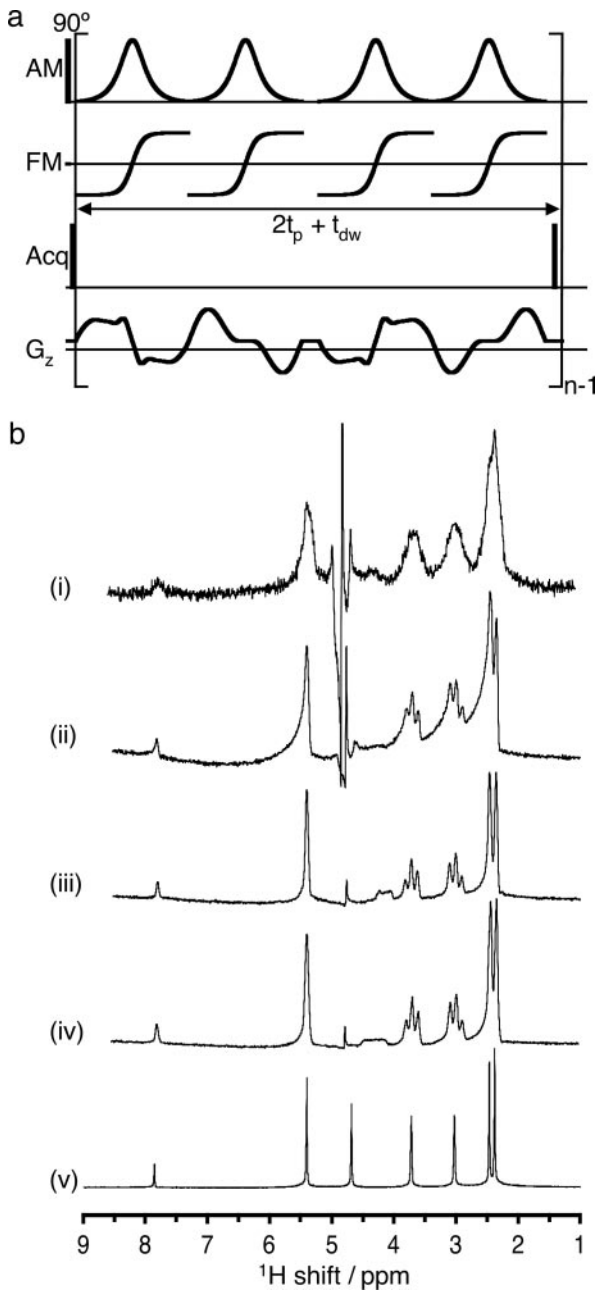

Fig. 2. NMR spectrum correction using shim pulses. (*a*) Pulse sequence for recording 1D NMR spectra with shim pulses applied between each point detected in the time domain signal. The total gradient waveform is a superposition of a constant baseline yielding the linear correction, and a smoothly modulated waveform, being numerically optimized to give a quadratic correction. We recorded $n = 1{,}024$ time-domain points stroboscopically during windows in a pulse train of shim pulses with length $t_p = 2$ ms and RF sweep width 40 kHz. The shim pulses were applied in pairs with opposite modulation polarity for increased robustness. Effective chemical-shift evolution takes place during a time $t_{dw} = 150$ μs for each detected point. (*b*) The ^{1}H NMR spectra for vitamin B_1 in ^2H_2O recorded with the pulse sequence shown in *a*. Inhomogeneous magnetic field without applied gradients (*i*), inhomogeneous magnetic field with linear correction (*ii*), inhomogeneous magnetic field with linear and quadratic correction (*iii*), homogeneous magnetic field without applied gradients (*iv*), and spectrum obtained with a simple 90° acquire experiment (*v*) are shown. The experimental artifacts of 4–5 ppm originate from partially suppressed $^1H^2HO$ and nonadiabatic transitions. The spectra are scaled to equal maximum intensity of the peak at 5.4 ppm. On an absolute intensity scale, the peak amplitudes in *i* are a factor of three smaller than in *iii*, whereas the intensities in *iii* and *iv* are comparable. The expanded triplet pattern for the peaks at 3.0 and 3.7 ppm in *i–iv* originates from evolution of *J* couplings during the shim pulses.

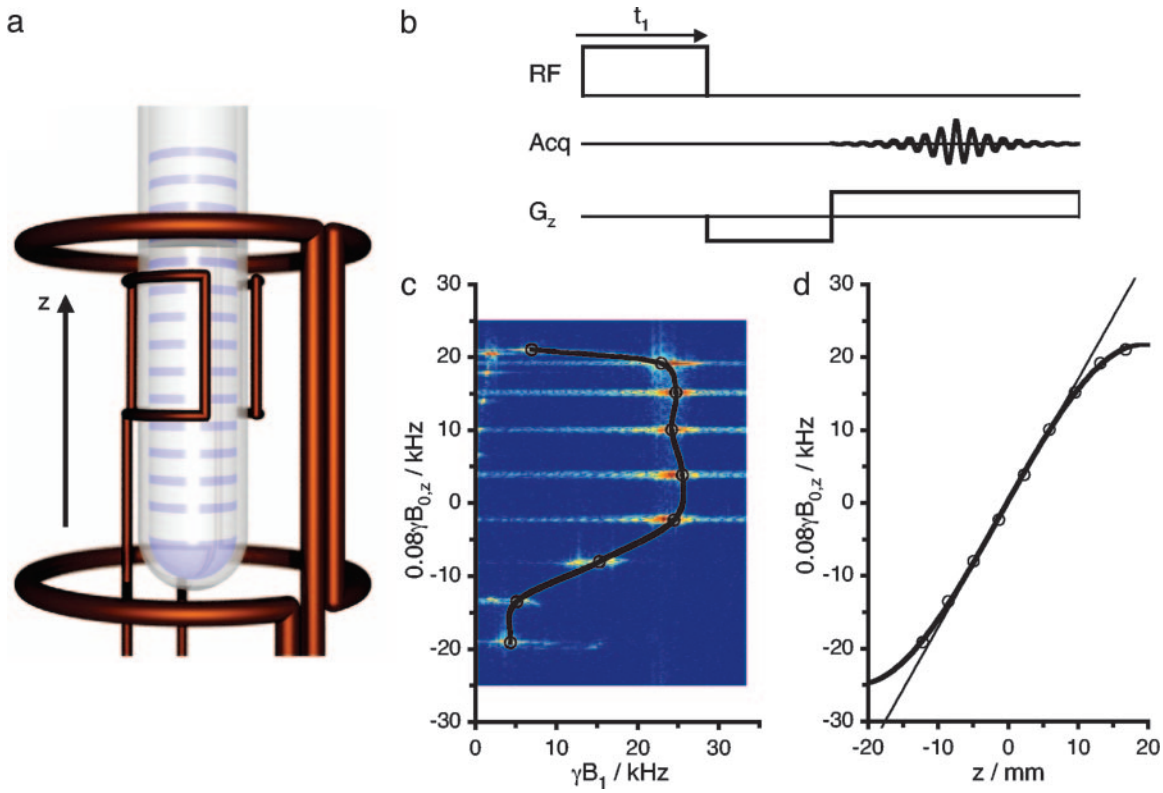

Fig. 3. RF and gradient field mapping. (*a*) Schematic experimental setup for a sample in a region of space with nonlinear field gradient. The RF coil (inner) is located off the center of the *z*-gradient coil (outer). Water located in grooves (1.25 mm deep and equally spaced 2.5 mm apart) cut into a Delrin rod gives rise to an NMR signal. (*b*) Pulse sequence for determining the correlation between the RF field B_1 and gradient field $B_{0,z}$. The NMR signal is recorded in the presence of the $B_{0,z}$ field as a function of the excitation pulse length t_1. The gradient amplitude was 8% of the maximum available value. A 2D Fourier transform yields the data shown in *c* from which $B_1(z)$ and $B_{0,z}(z)$ can be extracted. Circles indicate the 2D peaks, and the line is a smooth fit to guide the eye. (*d*) Experimental $B_{0,z}(z)$ (circles) and a fit of a third order polynomial (thick line). The thin line is an extrapolation of the linear field in the center of the gradient coil. The shim pulses were optimized for the region -3 mm $< z <$ 15 mm.

made inhomogeneous by using an x^2–y^2 shim coil, although the main field is homogeneous and we only use x and y gradient coils.

Shimming a Quadratic Magnetic Field Inhomogeneity Using a Linear Gradient. As a second demonstration, we use the shim-pulse methodology to correct the line broadening from an inhomogeneous magnetic field with linear and quadratic components by using a coil producing a linear magnetic field. Effective (i.e., nonrefocused) chemical shift evolution takes place during a delay of length t_{dw} between the individual shim pulses. The shim pulse should induce a phase shift that exactly cancels the evolution in the inhomogeneity during t_{dw}. The conditions for which the shim pulse was optimized can be stated as follows:

$$\begin{aligned} B_0(r) &\propto z + az^2 \\ B_{0,z}(\mathbf{r}) &\propto z \\ \phi(\mathbf{r}) &= -\gamma B_0(\mathbf{r}) t_{dw}, \end{aligned} \qquad [8]$$

where a is a constant. The current modulation was optimized for the quadratic part of the inhomogeneity making use of symmetry arguments to make the pulse scalable and improve the offset independence. When this modulation is added to a constant baseline current, simultaneous linear and quadratic corrections are possible.

The sample was 5 mg/ml thiamine (vitamin B_1) hydrochloride (purchased from Sigma–Aldrich and used without further purification) in ^2H_2O in a standard 5-mm o.d. sample tube. Accumulating 64 transients by using a recycle delay that was short in comparison with the relaxation time of water suppressed the signal from the residual $^1H^2HO$. A limited amount of sample was used to assure RF homogeneity. NMR spectra were recorded with the pulse sequence shown in Fig. 2*a*. The experimental spectra are shown in Fig. 2*b*. The spectrum obtained with inhomogeneous B_0 without applied gradients (Fig. 2*bi*) has a poor signal-to-noise ratio and does not reveal the fine structure. A constant current corrects for the z^1 term of the inhomogeneity, yielding a spectrum with highly asymmetric peaks (Fig. 2*bii*), which are typical for a z^2 inhomogeneity. With full current modulation, as shown in the pulse sequence in Fig. 2*a*, the homogeneous spectrum is recovered (Fig. 2*biii*). The spectra recorded in a homogeneous field with the adiabatic pulse train (Fig. 2*biv*), and with a one-pulse experiment (Fig. 2*b*), are shown for comparison. Note that all spectra in Fig. 2*b*, except *v*, are recorded with the adiabatic RF pulses an, thus, suffer from the same relaxation-induced line broadening (≈50 Hz). The different effective time scales for the sampling of chemical shifts and J couplings (chemical shift evolution is refocused at the end of the pulse, whereas the evolution of J couplings is not) leads to the expanded multiplet patterns for shim pulses in comparison with standard detection, as can be seen by comparing the peaks at 3.0 and 3.7 ppm in the spectra shown in *iv* and *v*.

Linearizing a Gradient with Linear and Cubic Components. The final example consists of correcting the image obtained with a setup in which the gradient coil produces a nonlinear gradient. A schematic representation of the experimental setup is shown in Fig. 3*a*. The RF coil is located at the edge of the gradient coil and, thus, will pick

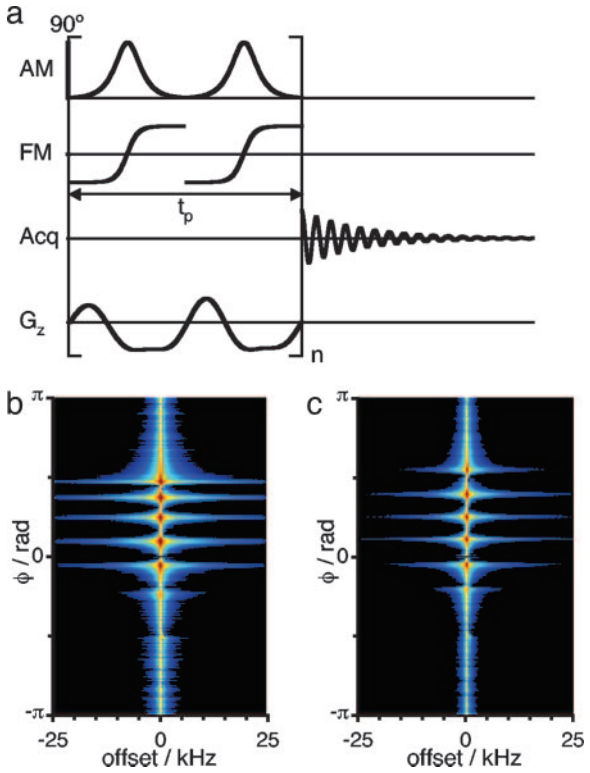

Fig. 4. NMR imaging using shim pulses. (*a*) Pulse sequence for recording a 2D correlation between offset and phase shift ϕ induced by the shim pulses. In the direct dimension, the signal is recorded during free precession in the main magnetic field. In the indirect dimension, n is incremented from 1 to 256. Experimental results for the geometry in Fig. 3 are shown for the case with $\phi(z) \propto B_{0,z}(z) \propto z - az^3$ (*b*) and $\phi(z) \propto z$ (*c*). Equal distance between the peaks implies that phase shift is proportional to position.

up signal from regions with nonlinear gradients. The sample was water in 1.25-mm-deep grooves cut in a Delrin rod (o.d., 4 mm). The correlation between $B_1(z)$ and $B_{0,z}(z)$ was estimated with the pulse sequence shown in Fig. 3*b*. Because the sample gives rise to signal from well defined positions along z, $B_1(z)$ and $B_{0,z}(z)$ can be estimated from the peak positions shown in Fig. 3*c*. The five peaks with $\gamma B_1 \approx 25$ kHz correspond to the grooves within the active volume of the RF coil. The compressed distance between the upper peaks results from the smaller gradient strength at the edge of the gradient coil. Above the RF coil, the gradient even reverses direction and $B_{0,z}(z)$ starts to decrease. The experimental $B_{0,z}(z)$ is shown in Fig. 3*d*, together with the fit of a third-order polynomial.

The shim pulse was optimized for the range of z containing the five grooves with an almost-constant B_1. To a good approximation, the pulse-design problem can be stated as follows:

$$B_{0,z}(\mathbf{r}) \propto z - az^3$$
$$\phi(\mathbf{r}) \propto z, \qquad [9]$$

where a is a constant. Images using shim pulses for phase encoding were recorded with the pulse sequence shown in Fig. 4*a*. Results for a shim pulse with $\phi(z) \propto B_{0,z}(z)$, which was used as a starting point for the iterative pulse design, and for an optimized shim pulse with $\phi(z) \propto z$ are shown in Fig. 4 *b* and *c*, respectively. The compressed distance between the peaks in the top part of Fig. 4*b* is similar to the results in Fig. 3*c*. This compression is corrected in Fig. 4*c*, demonstrating the ability to "linearize" imperfect gradient fields through the use of the shim-pulse methodology.

Discussion

The experiments reported above demonstrate that the shim-pulse approach is efficient in apparently reshaping the fields produced by the gradient coils. In principle, coils producing constant gradient fields in three orthogonal directions are, when operated in "shim-pulse mode," capable of reproducing the fields created by the higher-order shim coils in a modern high-field NMR magnet. The drawback is the finite duration of the shim pulse, on the order of 1 ms, which inevitably leads to signal loss because of relaxation and diffusion. The time-domain signal damping corresponds to a broadening of the resonance lines in the frequency domain. Thus, the shim-pulse methodology can never compete with a traditional shim stack if the only criterion is the spectral resolution. Relaxed hardware requirements and more volume available for the sample are factors favoring the shim pulses: three coils are obviously less voluminous than the traditional bulky shim stack. For certain applications, such as simple chemical analysis for industrial purposes, the requirement for perfect resolution is less crucial. A resolution of 1 ppm is sufficient to distinguish between small molecule components with reasonable chemical-shift dispersion. This methodology could be useful in applications such as quality control in the chemical industry. An inexpensive NMR system using shim-pulse technology could be used to determine whether a particular reaction product has been formed and whether known impurities are present. This type of system could also be used in the food industry to measure the relative amounts of components, such as water and fat. Another potential extension of this method could be used for high-throughput sample screening in an industrial or pharmaceutical setting. With the appropriate probe design, gradient selection and shim pulses could be used to enlarge the usable sample region of a traditional superconducting magnet. Several samples could potentially be loaded into a magnet and then sequentially examined, reducing the time needed for changing samples. It is likely that adequate resolution could be achieved with considerably simpler, smaller, and cheaper hardware if the flaws of the geometry of the coils were corrected by operating them in shim-pulse mode.

An exciting extension would be to combine the shim pulses with the *ex situ* methodology for acquiring resolved NMR spectra with inside-out or single-sided magnets. The current *ex situ* technique has the drawback of requiring a spatial matching between the B_1 field and the B_0 inhomogeneity. Inhomogeneous fields with some matching between the B_1 and B_0 fields are inherent in the single sided-design: both fields decay away from the coils, which are in spatial proximity to each other in all reasonable designs. However, the symmetry of the fields are completely different for currently existing equipment, such as the NMR-MOUSE (14). Better matching can quite easily be achieved if the matching is taken into account during the coil design. A set of auxiliary B_0 coils operating in shim-pulse mode could also relax the requirement for perfect field matching. For single-sided imaging applications, such coils are already used for traditional phase encoding (15, 16).

Conclusions

We have demonstrated the feasibility of using shim pulses to make the spins behave as though they were precessing in a magnetic field of a different shape than the ones produced by the hardware components. The shape of the apparent field is controlled by the time modulation of the RF field and gradient coil currents. The shim-pulse methodology can be used to make the field from less-than-perfect hardware components appear to be homogenous for spectroscopy or to have a constant gradient for imaging.

This work was supported by the Office of Science, Basic Energy Sciences, U.S. Department of Energy Contract DE-AC03-76SF00098. R.W.M. was supported by Department of the Army Contract DAMD 17-03-1-0476. D.T. was supported by a postdoctoral fellowship grant from the Swedish Research Council.

1. Meriles, C. A., Sakellariou, D. & Pines, A. (2003) *J. Magn. Reson.* **164,** 177–181.
2. Meriles, C. A., Sakellariou, D., Heise, H., Moulé, A. J. & Pines, A. (2001) *Science* **293,** 82–85.
3. Heise, H., Sakellariou, D., Meriles, C. A., Moulé, A. J. & Pines, A. (2002) *J. Magn. Reson.* **156,** 146–151.
4. Sakellariou, D., Meriles, C. A., Moulé, A. J. & Pines, A. (2002) *Chem. Phys. Lett.* **363,** 25–33.
5. Sakellariou, D., Meriles, C. A. & Pines, A. (2004) *C. R. Phys.* **5,** 337–347.
6. Demas, V., Sakellariou, D., Meriles, C. A., Han, S., Reimer, J. & Pines, A. (2004) *Proc. Natl. Acad. Sci. USA* **101,** 8845–8847.
7. Frydman, L., Scherf, T. & Lupulescu, A. (2002) *Proc. Natl. Acad. Sci. USA* **99,** 15858–15862.
8. Shapira, B., Lupulescu, A., Shrot, Y. & Frydman, L. (2004) *J. Magn. Reson.* **166,** 152–163.
9. Shrot, Y. & Frydman, L. (2004) *J. Magn. Reson.* **167,** 42–48.
10. Shapira, B. & Frydman, L. (2004) *J. Am. Chem. Soc.* **126,** 7184–7185.
11. Hürlimann, M. D. (2001) *J. Magn. Reson.* **148,** 367–378.
12. Garwood, M. & DelaBarre, L. (2001) *J. Magn. Reson.* **153,** 155–177.
13. Baum, J., Tycko, R. & Pines, A. (1985) *Phys. Rev. A* **32,** 3435–3447.
14. Blümich, B., Blümler, P., Eidmann, G., Guthausen, A., Haken, R., Schmitz, U., Saito, K. & Zimmer, G. (1998) *Magn. Reson. Imaging* **16,** 479–484.
15. Perlo, J., Casanova, F. & Blümich, B. (2004) *J. Magn. Reson.* **166,** 228–235.
16. Brown, M. C. A., Verganelakis, D. A., Mallett, M. J. D., Mitchell, J. & Blümler, P. (2004) *J. Magn. Reson.* **169,** 308–312.